Effect of Fiber Dispersion on Broadband Chaos Communications Implemented by Electro-Optic Nonlinear Delay Phase Dynamics

Romain Modeste Nguimdo, *student member OSA*, Roman Lavrov, Pere Colet, *member IEEE, OSA*, Maxime Jacquot, Yanne Kouomou Chembo and Laurent Larger

Abstract— **We investigate theoretically and experimentally the detrimental effect of fiber dispersion on the synchronization of an optoelectronic phase chaos cryptosystem. We evaluate the root-mean square synchronization error and the cancellation spectra between the emitter and the receiver in order to characterize the quality of the optical fiber communication link. These two indicators explicitly show in temporal and spectral domain how fiber dispersion does negatively affect the phase chaos cancellation at the receiver stage. We demonstrate that the dispersion management techniques used in conventional optical fiber networks, such as dispersion-compensating modules/fibers or dispersion shifted fibers, are also efficient to strongly reduce the detrimental effects of fiber propagation in phase chaos communications. This compatibility therefore opens the way to a successful integration of more than 10-Gb/s phase chaos communications systems in existing networks, even when the fiber link spans over more than 100 km.**

Keywords— **Phase modulation, optical communications, chaos cryptography, synchronization, nonlinear systems.**

I. Introduction

CHAOS communication systems require the use of transmitters and receivers operating in synchronized chaotic regime, even if located far one from another [1]. For optical fiber communication networks, the chaotic masking motion used for encryption is carried by a laser beam and this optical chaos can be generated using a wide variety of architectures (see refs. [2], [3] and references therein). In a recently proposed efficient and fast optical phase dynamics [4], [5], chaos is generated by combining electro-optical phase modulation, an external nonlinear phase-to-intensity converter, and a delay induced by an optoelectronic feedback loop (fiber, RF photodetectors, and amplifier).

As any communication system, chaos cryptosystems have to overcome the problem of signal-to-noise ratio at the receiver stage. In our case, this noise mainly arises from three different sources. The first source is constituted by the unavoidable stochastic fluctuations that are affecting the system; in order to minimize its influence, there is no other solution than to use optoelectronic components that are the less noisy possible. The second source is specific to chaos cryptosystems, and it is due to the various mismatches in parameters between the emitter and the receiver [6], [7], [8]. Theoretically, for an open loop self synchronizing scheme, this noise vanishes when the emitter and the receiver are identical; but in practice, reducing this noise to a minimum requires a careful matching of the system components, or (in marginal cases) a fine tuning leading to a partial mismatch compensation [7]. The third source of noise of noise will be the main purpose of this article; it arises from the encrypted signal distortion due to transmission over the communication channel. Effectively, the carrier is subjected to attenuation, Kerr nonlinearity and chromatic dispersion during its propagation in the fiber. The latter effect is in our case the most damaging, because the encrypted signal bandwidth may span over more than 30 GHz around the nominal frequency of the laser beam. Hence, dispersion shuffles this broadband spectrum and as a consequence, synchronization noise arises because of imperfect phase chaos replication at the receiver. This residual cancellation noise is naturally expected to increase with the spectral bandwidth of the signal, with the length of the fiber link, and with the absolute value of the chromatic dispersion. It is however interesting to note that from a communication engineering point of view, phase (or frequency) modulation schemes are more robust than their amplitude/intensity modulation counterparts, so one may expect that a chaotic phase modulation cryptosystem could yield improved chaos synchronization results relatively to earlier architectures where optical intensity chaos modulation was implemented and operated in real world networks [3]. In fact, the results reported here indicate a better synchronization performance when compared with previous measurements in electro-optical intensity chaos [9]. To the best of our knowledge, very few investigations have been devoted to the topic of fiber propagation effects on the performance of chaos cryptography [10], [11], [12], [13], and they were exclusively based on numerical simulations. Fiber transmission has been considered in some experimental works [3], [14], but no detailed analysis on the fiber dispersion effects has been reported. Our aim in this paper is to address this issue with a joint theoretical and experimental analysis, and with a particular emphasis on the exploration of various dispersion management schemes able to minimize the detrimental effects of chromatic dispersion.

R. M. Nguimdo (email: modeste@ifisc.uib.es) and P. Colet are with the Instituto de Física Interdisciplinar y Sistemas Complejos, IFISC (UIB-CSIC), Campus Universitat de les Illes Balears, E-07122 Palma de Mallorca, Spain. R. Lavrov, M. Jacquot, Y. K. Chembo and L. Larger are with the Optics Department, FEMTO-ST Institute (UMR CNRS 6174), 16 Route du Gray, 25030 Besançon cedex, France.

The authors acknowledge financial support from the European Community (PICASSO project, FP6-2006-IST-2.5.1) and from MICINN, Spain, and Feder under Project TEC2006-1009/MIC (PhoDECC) and Project FIS2004-00953 (CONOCE2). R.M.N. also acknowledges the fellowship BES-2007-14627 under the FPI program of MICINN (Spanish Government).

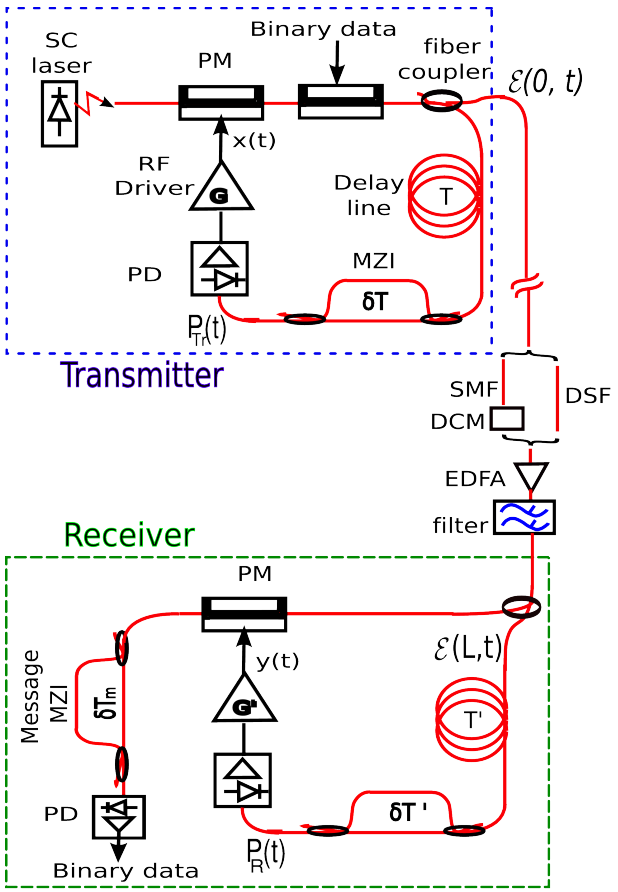

Fig. 1. Experimental setup. EDFA: erbium-doped fiber amplifier; MZI: Mach-Zehnder interferometer; PD: photodiode; PM: phase modulator; SL: semiconductor laser; SMF: Single Mode Fiber, DCM: Dispersion Compensation Module DSF: Dispersion Shifted Fiber.

The paper is organized as follows. In Sec. II, we present the system under study and we show how the message encoding/decoding is performed. The Sec. III is devoted to the study of cancellation (or synchronization) noise, while Sec. IV is dedicated to the corresponding spectra. The last section summarizes our results and concludes the article.

II. The system

The schematic representation of the communication system under study is shown in Fig. 1. It is inspired by the work presented in ref. [4], [5], where the concept of nonlocal nonlinearity has been defined for chaos generation, as a consequence of the use of an imbalanced interferometer for performing nonlinear phase to intensity demodulation. Three sub-systems can be distinguished: the transmitter, the channel, and the receiver. They are described in details in the next subsections.

A. Transmitter

The transmitter performs two operations: it encodes into the optical domain an original binary message through a classical differential phase shift keying electro-optic modulation. This optical phase modulation is subsequently hidden within a broadband noise-like phase modulation, which is obtained through the principle of nonlocal nonlinear delay phase chaos generation.

The transmitter thus consists of a continuous-wave distributed feedback semiconductor laser feeding a $LiNbO_3$ phase modulator with the wavelength $\lambda = 2\pi c/\omega_0 = 1.55\ \mu$m. This phase modulator having a halfwave voltage of V_π, receives the electrical chaotic input from a broadband radio-frequency (RF) driver, and translates this electrical signal modulation into the optical phase one while keeping the intensity unchanged. The optical phase therefore changes proportionally to the voltage applied to the modulator, and the time dependent phase shift introduced by the modulation is

$$\varphi(t) = \pi \frac{V(t)}{V_\pi}\,. \tag{1}$$

The message is mixed with the chaos through a second cascaded phase modulator, which is assumed for simplicity to have the same V_π. The message phase modulation is performed by driving the modulator with a V_π peak-to-peak voltage in order to add a π phase shift, following the standard differential phase shift keying (DPSK) modulation scheme. Hence, the encoded message introduces in practice an additional phase shift, so that the total optical phase at the output of the message phase modulator reads:

$$\psi(t) = \pi \frac{V(t)}{V_\pi} + \pi \frac{\mu(t)}{V_\pi}\,, \tag{2}$$

where $\mu(t) = \pm V_\pi$ is the message amplitude.

The electric field has only one vectorial polarization in our system, so that we can restrict ourselves to a scalar description of the optical field. The output is split into two parts, one is transmitted through the channel while the other enters in the delay line. The complex envelope of the electric field can be written as $\mathcal{E}(z,t)$, where z is the distance from the output of the message phase modulator, and t is time. For the transmitted part the dependence on z is taken into account in the next subsection dealing with fiber propagation. For the part going through the emitter loop we neglect any dependence on z since the effects of the fiber propagation within the transmitter are negligible. From Eq. (2), one has

$$\mathcal{E}(0,t) = E_0 \exp\left[i\psi(t)\right]\,, \tag{3}$$

where $i^2 = -1$ and E_0 is the field amplitude. This envelope is then delayed by a time T while traveling through the optical feedback path in the transmitter. This optical signal subsequently crosses an imbalanced Mach-Zehnder interferometer (MZI) that performs a nonlinear phase-to-intensity conversion. This conversion is led by the mean of a nonlocal nonlinearity in time, since it is ruled by an intrinsic differential delay which is significantly greater than the typical phase variations timescale. The MZI imbalance is also responsible for an extra constant phase $\omega_0 \delta T$ of the interference condition, which corresponds to the static operating point of the nonlinear conversion. In practice, this offset phase is strongly sensitive to environmental fluctuations, and it needs to be actively controlled through a fine

tuning of δT (e.g. thermal control between the imbalanced arms of the interferometer): the chaotic masking thus remains deterministic and controllable, which is a required condition for proper chaos replication at the receiver side. It should be noticed here that a standard DPSK demodulator was used for experimental convenience as a nonlinear phase-to-intensity converter. In a practical chaos encryption system, one would probably prefer a more complex and dedicated similar device than a standard MZI, consisting for example in a multiple arms imbalanced interferometer. The physical parameters defining the dynamic and static conditions of each interferometer arm would represent an additional customized secret key of the hardware encryption.

The optical intensity at the MZI output is thus a nonlinear nonlocal transformation of the phase modulation:

$$P_{\mathrm{Tr}}(t) = P_0 \cos^2\left\{\frac{1}{2}\left[\omega_0 \delta T + \psi(t-T) - \psi(t-T-\delta T)\right]\right\}, \tag{4}$$

where $P_0 = |E_0|^2/(\mu_0 c)$, μ_0 being the vacuum permeability and c the speed of the light. This optical intensity is then converted to the electrical domain by a photodiode. This electrical signal is thus band-pass filtered by the electronics of the feedback loop, which RF frequency filtering process can be modelled in the time domain by an integro-differential operator characterized by a high- and a low-frequency cut-off. For sake of simplicity we assume that the filter is linear and of second order, so that the dynamics of the input RF voltage at the input of the chaos phase modulator obeys

$$V(t) + \tau \frac{dV}{dt}(t) + \frac{1}{\theta}\int_{t_0}^{t} V(s)ds = \eta G_0 S P_{\mathrm{Tr}}(t)\,, \tag{5}$$

where θ and τ are the characteristic response times attached to the low and high cut-off frequencies of the filter respectively, G_0 stands for the amplifier gain, η accounts for overall optical losses, and S is the photodetection efficiency. Note that the condition $\tau \ll \theta$ has been taken into account in the above equation (easily fulfilled assumption, since the feedback filtering is broadband for telecom devices). For mathematical convenience we introduce the dimensionless variables $x(t)$ and $m(t)$ as follows:

$$x(t) = \pi \frac{V(t)}{2V_\pi} \equiv \frac{\varphi(t)}{2}\,, \tag{6}$$

$$m(t) = \pi \frac{\mu(t)}{2V_\pi}\,, \tag{7}$$

so that Eq. (5) can be rewritten in the dimensionless form as

$$x(t) + \tau \frac{dx}{dt}(t) + \frac{1}{\theta}\int_{t_0}^{t} x(s)ds = G\cos^2\left\{x(t-T) - x(t-T-\delta T) + m(t-T) - m(t-T-\delta T) + \Phi_0\right\}, \tag{8}$$

where $G = \pi\eta G_0 S P_0/(2V_\pi)$ is the overall feedback loop gain, and $\Phi_0 = \omega_0 \delta T/2$ is a constant offset phase. This equation rules the dynamics of the input RF voltage at the first phase modulator.

B. Optical channel

According to the experimental setup shown in Fig. 1, the light beam launched into the fiber communication channel corresponds to the optical signal at the second phase modulator output. The transmitter modeling of Eq. (2) allows to derive the electric field envelope of that transmitted light as being expressed by:

$$\mathcal{E}(0,t) = E_0 \exp\left\{2i[x(t) + m(t)]\right\}\,. \tag{9}$$

The propagation on the fiber can be described in the moving frame by [15]:

$$\begin{aligned}\frac{\partial \mathcal{E}}{\partial z}(z,t) &= -\frac{\alpha}{2}\mathcal{E}(z,t) - i\frac{\beta_2}{2}\frac{\partial^2 \mathcal{E}}{\partial t^2}(z,t) + \frac{\beta_3}{6}\frac{\partial^3 \mathcal{E}}{\partial t^3}(z,t) \\ &\quad + i\gamma\left|\mathcal{E}(z,t)\right|^2 \mathcal{E}(z,t),\end{aligned} \tag{10}$$

where β_2 is the second order dispersion, β_3 is the third order dispersion, γ is the nonlinear Kerr factor and α is the linear attenuation. As discussed later, two setups are being considered, one including single mode fiber plus dispersion compensation and another considering a dispersion shifted fiber. After propagating $\mathcal{E}(0,t)$ over a distance $L \leq 50$ Km (and eventually going through dispersion compensation) the output is amplified to compensate for the losses. Experimentally amplification is realized by an EDFA followed by an optical channel filter that removes most of the spontaneous emission noise introduced by the EDFA, therefore in the numerical simulation we consider a noiseless amplifier.

C. Receiver

In a symmetric way with respect to that described for the transmitter, the receiver stage does simultaneously undertake two distinct actions: chaos cancellation, and DPSK message demodulation. The receiver input light is split into two parts using a variable coupler: one part is sent to a nonlinear delay processing branch, while the second part is fed into the local electro-optic phase modulator which role is to remove electro-optically the chaotic phase encryption mask. The amplifier and the variable coupler are set in such a way that the field going into the delay $\mathcal{E}(L,t)$ branch has the same mean power P_0 as in the transmitter. In the case of an ideal chaos cancellation, the receiver phase modulation output therefore corresponds to a standard DPSK-modulated light beam (the one imposed by the message phase modulator in the transmitter). The modeling of chaos cancellation can be described following a similar approach as previously done for the emitter. The optical field arriving at the MZI is $\mathcal{E}(L, t-T_R)$, so the MZI intensity output is

$$P_{\mathrm{R}}(t) = \frac{1}{\mu_0 c}\frac{1}{4}\left|\mathcal{E}(L,t-T')e^{i(2\Phi_0' + \pi)} + \mathcal{E}(L,t-T'-\delta T')\right|^2 \tag{11}$$

where the prime (') indicates the receiver parameters. In order to remove the chaotic masking, the replicated chaos needs to have the opposite sign with respect to the emitter one. This is easily achieved experimentally operating

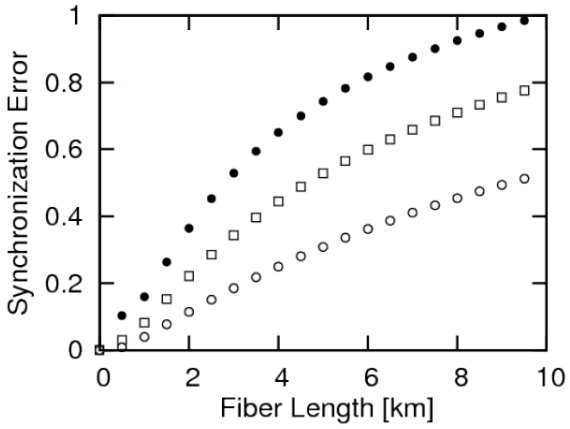

Fig. 2. Numerical simulation of the synchronization error between the emitter and receiver as a function of fiber length in a standard SMF with $\beta_2 = 20$ ps^{2}km^{-1} and $\beta_3 = 0$. The various values of the feedback gains are $G = 2.5$ ($\circ$), $G = 3.5$ ($\square$), and $G = 5.0$ ($\bullet$).

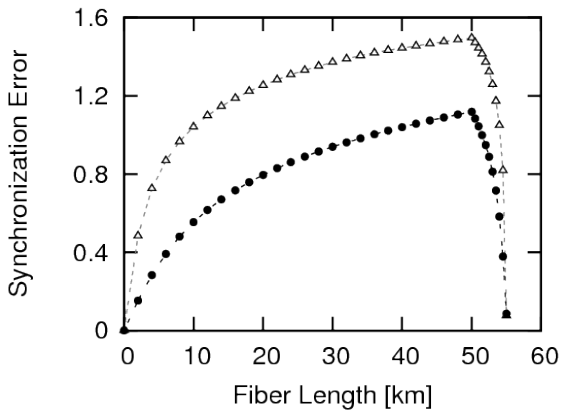

Fig. 3. Numerical simulation of the dispersion compensation using DCFs with $\beta_{2\mathrm{DCF}} = -200$ ps^2/km $\beta_{3\mathrm{DCF}} = 0.1$ ps^3/km, $\alpha_{\mathrm{DCF}} = 0.6$ dB, $\gamma_{\mathrm{DCF}} = 6$ W^{-1}km^{-1}. The values used for the feedback gains are $G = 2.5$ ($\bullet$) and $G = 5.0$ ($\triangle$). When the chaotic carrier is launched at $z = 0$, the synchronization error increases steadily but at $z = 50$ km, a 5 km-long DCF is used and drastically reduces the cancellation noise.

the MZI with a $\pi-$shifted static phase as indicated in Eq. (11). Alternatively this could have been done using balanced photodiodes and exchanging their inputs or using an inverted amplifier at the receiver.

Under such conditions the normalized signal $y(t)$ driving the receiver phase modulator with an anti-replica of the chaotic masking, is ruled by the following "open loop" dynamics:

$$y(t) + \tau' \frac{dy(t)}{dt} + \frac{1}{\theta'} \int_{t_0}^{t} y(s)ds = G' \frac{P_R(t)}{P_0}\,. \qquad (12)$$

where $G' = \pi\eta' G'_0 S'/(2V'_{\mathrm{R}\pi})$

The receiver electro-optic phase modulator applies an additional phase modulation onto the received light beam, proportionally to the signal $y(t)$. This leads to a total optical phase modulation proportional to $(x+y)$ at the chaos cancellation output. When a DPSK message modulation is applied at the transmitter, this sum is intended to retrieve the DPSK modulation only, the one proportional to $m(t)$, due to the anti-phase chaos replica expected for $y(t)$. The resulting light beam can then be processed through a standard DPSK demodulator matched with the message bit rate (imbalanced MZI with δT_m in Fig.1). The photodiode detects

$$\mu_R(t) = \frac{1}{4} S \left| \mathcal{E}(L,t) e^{2iy(t)} + \mathcal{E}(L, t-\delta T_m) e^{2iy(t-\delta T_m)} \right|^2 . \qquad (13)$$

In the absence of a binary DPSK message, the sum $\varepsilon = (x + y)$ is used to evaluate the accuracy of the phase chaos cancellation. Similarly to the usual signal-to-noise ratio, a cancellation-to-chaos ratio can be defined in order to analyze the accuracy of the chaos cancellation in a normalized way.

III. Numerical results: cancellation noise

In this section, we theoretically investigate the time-domain variations of the cancellation noise when the fiber and the chaotic carrier parameters are varied. This analysis relies on the coupled Eqs. (8), (10) and (12) with the parameters $\tau = 20$ ps, $\theta = 1.6$ μs, $\delta T = 0.4$ ns, $\Phi_0 = \pi/4$ and $T = 70$ ns. The power P_0 is 5 mW, and we consider a single mode fiber (SMF) for the transmission channel, with parameters $\beta_2 = 20$ ps^2 km^{-1}, $\beta_3 = 0.1$ ps^2 km^{-1}, $\gamma = 1.1$ W^{-1}km^{-1}, $\alpha = 0.2$ dB km^{-1} (0.046 km^{-1}). The propagation of the optical signal in the optical fiber channel is simulated using the split-step Fourier algorithm, while the calculation of the emitter receiver dynamics is performed using the predictor-corrector algorithm. The influence of parameter mismatch has already been explored elsewhere [7] for a similar electro-optic chaos communication system, so that we can here concentrate on the effects of the fiber channel only. In this section all the receiver parameters will thus be assumed to be perfectly matched in the receiver. This hypothesis enables an easier understanding of the cancellation noise that is exclusively due to fiber propagation effects. Without any message inserted, we characterize the system performance using the normalized cancellation-to-chaos ratio defined as

$$\sigma = \sqrt{\frac{\langle \varepsilon^2(t) \rangle}{\langle x^2(t) \rangle}}\,. \qquad (14)$$

We remark that the perfect cancellation of the chaos is expected when $y(t)$ perfectly anti-synchronizes with $x(t)$.

Figure 2 illustrates clearly the dramatic influence of the fiber channel on the chaos cancellation at the receiver, when SMF only is involved in the optical link. The situation worsens as expected for higher feedback strength ($G = 5.0$), as this corresponds to an even broader chaotic spectrum to be conveyed through the dispersive channel (thereby it increases the linear frequency mixing effect of dispersion). For each situation reported in Fig. 2, we clearly see that a strong signal distortion occurs already for propagation over 10 km only of SMF. In this case, the message could not be successfully retrieved because the synchronization error is too large. Typically, one would

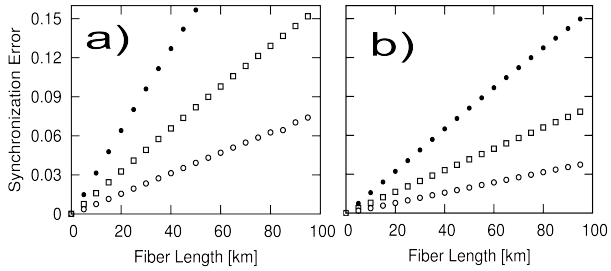

Fig. 4. Numerical simulation using DSFs. The values used for the gains are $G = 2.5$ (○), $G = 3.5$ (□), and $G = 5.0$ (●). (*a*) Synchronization error with the parameters $\beta_2 = 0.2$ ps^{2}km^{-1} and $\beta_3 = 0$. (*b*) Synchronization error with the parameters $\beta_2 = 0.1$ ps^{2}km^{-1} and β_3=0.1 ps^{3}km^{-1}.

expect this error to be below 10%, which is of the order of the best experimental cancellation-to-chaos ratio due to residual parameter mismatch in a back-to-back configuration [4].

Since the nonlinear effects are relatively weak in our context, the large distortion mainly originates from chromatic dispersion. This first result on a standard non compensated fiber channel shows that phase chaos communication is requiring necessarily a proper management of the dispersion effects.

A. Using dispersion-compensation

Dispersion can be compensated either using a Dispersion Compensation Module (DCM) or a Dispersion Compensating Fiber (DCF). We model here the later. Generally, a DCF has a negative dispersion with nominal values which are typically ten times higher than those of the fiber to be compensated for, and attenuation in DCFs is usually higher as well. Therefore, in order to adequately compensate for the dispersion induced in the SMF, we consider the parameters $\beta_{2DCF} = -10\beta_2$, $\alpha_{DCF} = 3\alpha$ and $\gamma_{\rm DCF} = 6$ W^{-1}km^{-1}. Hence, after the propagation over a SMF with length L_1, the signal is launched into a DCF with length $L_2 \ll L_1$, and which satisfies the condition

$$\beta_2 L_1 + \beta_{2DCF} L_2 = 0\,. \tag{15}$$

In Fig. 3, the chaotic carrier undergoes distortion after traveling over $L_1 = 50$ km of SMF, and then is launched into a DCF in which it goes back closer to its initial state. In the figure we plot what would be the synchronization error if a receiver was placed at a given point in the fiber. Synchronization error grows with the propagation distance until the DCF is reached, and then it decreases owing to the compensation. Finally for a 5 km compensation with DCF, one can obtain a synchronization error as small as 7.5% when considering a transmitter with $G = 5$. The situation is almost the same for smaller gain values ($G = 2.5$), where the synchronization error is also estimated to 7.5%. Hence, for DCFs, the compensation is almost independent of G. It is interesting to note that this residual synchronization error is exclusively due to the effect of the fiber nonlinearity, and the third order dispersion which remain

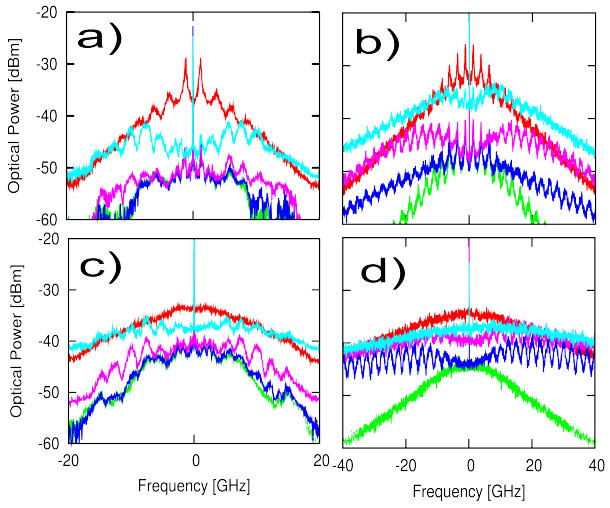

Fig. 5. (Color online) Experimental (a,c) and numerical (b,d) chaos cancellation spectra for transmission over standard SMF spools, with (a,b) $G = 2.5$ and (c,d) $G = 5.0$. Red: chaotic carrier; Green: back-to-back transmission; Blue: $L = 1$ km; Magenta: $L = 3$ km; Cyan: $L = 21$ km. The numerical results has been obtained considering a mismatch of 5% in τ and 10% in G.

uncompensated. Simulation results without the nonlinear term in Eq. (10) indeed yields a quasi-null synchronization error (below 0.5%), even if the 3rd order dispersion is not matched.

B. Using a dispersion-shifted fiber (DSF)

Another alternative way for the reduction of dispersion effects over a fiber channel is to use a DSF in which the second order dispersion is set close to zero, without modifying the other properties of the fiber. The results obtained with this method are displayed in Fig. 4, showing the evolution of the synchronization error when a carrier is transmitted through a DSF. In Fig. 4a, the broadest chaotic spectrum ($G = 5.0$) is still distorted, so that the synchronization error reaches 15% after a propagation over $L \sim 50$ km, with $\beta_2 = 0.2$ ps^{2}km^{-1}. If one manages to reduce the value of β_2 (e.g. down to 0.1 ps^{2}km^{-1}), better synchronization is achieved as shown in Fig. 4b, even when third order dispersion is considered (about 10% after 50 km, with the highest gain G). It can be noted that globally, the DSF compensation scheme is more efficient for lower gain values in Figs. 4a and 4b; the optimum has therefore to be found between increased security (requiring strong hyperchaos and a broad spectrum through a high gain) and increased signal-to-noise ratio (requiring a minimization of the cancellation noise).

IV. Experimental results: cancellation noise spectra

We have performed experimental measurements in order to evaluate the chaos cancellation level after propagation in optical fiber spools available in the laboratory. Chaos cancellation spectra measurements were chosen as indicators of the chaos communication link performance, in order to

have a relevant comparison between experiment and theory.

In order to improve the synchronization quality, additional 7.73 GHz low-pass filters (corresponding in the modeling to a slightly slower response time τ) have been added right after the photodiodes, as it is usually the case for 10 Gb/s data detection in optical communication networks. We expect thus that the width of the chaotic carrier is better matched to that of 10 Gb/s DPSK message spectrum (higher frequency chaotic spectral components would anyway not be useful for message masking at that bit rate). Our cancellation spectra are obtained with an optical spectrum analyzer (OSA) with 10 MHz resolution. For each chaos cancellation spectrum, we also recorded the corresponding chaotic spectrum without cancellation, so that the difference between the two situations can lead easily to the cancellation-to-chaos ratio in the spectral domain.

Figures 5 a), c) display several experimental cancellation spectra after propagation in standard SMFs. It is intended to evidence the degradation of chaos cancellation when dispersion effects grow with increase of the fiber length. As in Fig. 2, the varied parameters were the feedback loop gains and the fiber lengths. Numerical power spectral density of the optical field is shown in panels b), d) [16]. Figures 5 a), b) display the low gain case. A few peaks are easily recognizable in the carrier spectrum, thereby indicating that the full hyperchaotic regime (strong, flat, and broadband) has not been reached completely with such a gain. When the propagation length is low (0 and 1 km), the cancellation noise is globally higher than 20 dB (this figure can straightforwardly be considered as a kind of chaos-to-cancellation ratio). A degradation is observable when L is increased up to 3 km, and for a 21 km link, the chaotic carrier is not canceled at all beyond 7 GHz. For the highest achievable feedback gain $G = 5.0$ (Figure 5 c), the spectrum of the carrier is much smoother, as the full hyperchaotic regime is obtained. In this case, the cancellation performance is between 15 and 20 dB in the back-to-back configuration. However, the same degradation is witnessed as the fiber lengths increase. Hence, at this stage of the experimental study, it is clear that multi-Gb/s chaos cryptosystems cannot be operated in standard optical networks with SMFs beyond few kilometers without dispersion compensation, as the cancellation performance becomes severely degraded.

A. Using dispersion compensation modules (DCMs)

At the experimental level, we compensate the fiber dispersion through the utilization of DCMs. The principle of compensating with DCMs consists in propagating the carrier over a fiber length L_1, then launching it into the DCM which is adjusted so that the cancellation is the best possible. Even though DCMs are not exactly equivalent to the DCFs used in the numerical analysis in Sec. III-A, the underlying physical mechanism is very similar, at least for the second order dispersion phenomena.

In Figs. 6 a), c), a tunable dispersion compensation module with a wide bandwidth and a large control tuning range is used (TDCM from Teraxion). Very good cancellation

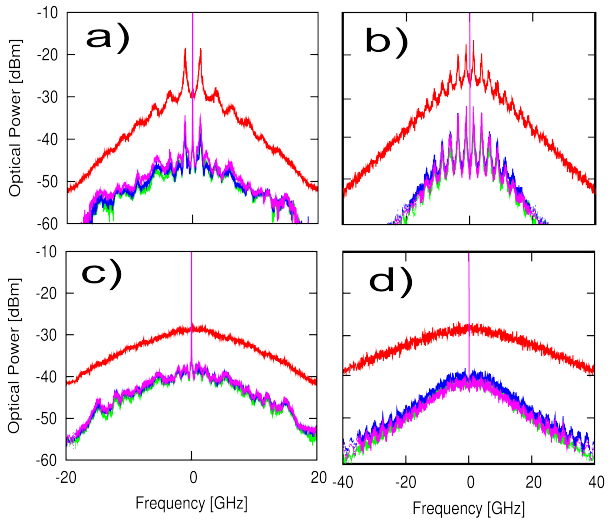

Fig. 6. (Color online) Experimental (a,c) and numerical (b,d) chaos cancellation spectra for transmission over SMF spools and using dispersion compensation. (a,b) $G = 2.5$ and (c,d) $G = 5.0$. Red: chaotic carrier; Green: back-to-back transmission, blue: $L = 20$ km of SMF; Magenta: $L = 50$ km of SMF. Numerical results has been obtained considering DCF as in Fig. 3 and a mismatch of 5% in τ and 10% in G.

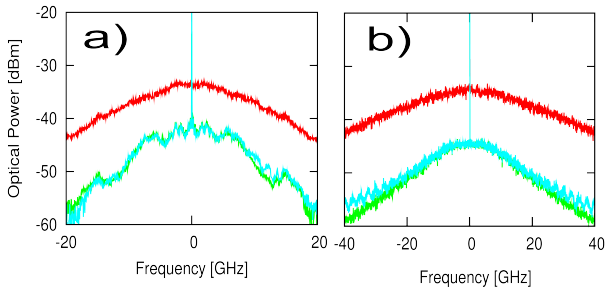

Fig. 7. (Color online) Experimental (a) and numerical (b) chaos cancellation spectrum for transmission over a 22 km-long DSF spool, with $G = 5.0$. Red: chaotic carrier; Green: back-to-back transmission; Cyan: $L = 22$ km. The numerical results has been obtained considering $\beta_2 = 0.1$ ps^{2}km^{-1}, β_3=0.1 ps^{3}km^{-1} and a mismatch of 5% in τ and 10% in G.

spectra is obtained by tuning DCM either to -360 ps/nm to compensate for a dispersion over 20 km of SMF or to -880 ps/nm for 50 km of SMF, independently of the feedback strength G . Typically, the use of DCMs is seen here as an excellent alternative at up to 50 km, as it enables to cancel almost completely the detrimental effects of fiber dispersion, with a weak penalty of the order of 1 dB (experimentally, the synchronization error, or equivalently the chaos cancellation level, is mainly dominated by unavoidable residual parameter mismatch). For comparison the numerical spectra using a DCF with parameters as in Fig. 3 and considering a mismatch of 5% in τ and 10% in G is shown in Figs. 6 b), d).

It should be noticed here that we can highlight an interesting issue of the dispersion sensitivity of phase chaos communication schemes. The use of DCM could indeed not only be efficient for channel dispersion compensation. Such

modules could also be involved inside the phase chaos generation feedback loop, for introducing additional system complexity and security. The dispersion value set at the transmitter would thus represent an additional secret key as a physical parameter, which would be required at the receiver with the right value, in order to achieve the actual phase chaos cancellation and the decoding of the chaotic masking.

B. Using dispersion-shifted fibers (DSFs)

Another solution that can be experimentally implemented is to use DSFs, exactly as in the numerical analysis of Sec. III-B. In Fig. 7, the measurement of DSF influence on transmission is reported. Though the operating wavelength (1562.0 nm) was slightly different from the zero-dispersion wavelength of the DSF fiber (1550.8 nm), dispersion was low enough so that after transmission over 22 km of fiber only small differences from the back-to-back case are seen in the cancellation spectrum. If compared with transmission over SMF without dispersion compensation (Fig. 5b), equally small distortion of the cancellation spectrum is observed only for the 1 km SMF case, while the effects of longer fibers are significantly more pronounced.

V. Conclusion

We have led a joint theoretical and experimental study to investigate the detrimental effects of fiber propagation on the synchronization of an optical phase-chaos emitter-receiver system separated by several tens of km, and potentially operating up to 10 Gb/s. We have shown that when propagating in standard SMFs, the broadband chaotic carriers are drastically affected by chromatic dispersion, and message recovery is impossible beyond few kilometers. We have explored two classical methods of dispersion management, namely dispersion compensation fibers/modules and dispersion-shifted fibers, in order to evaluate their suitability for optical chaos cryptosystems. Both numerical and experimental results have shown that the cancellation noise can be reduced down to the level of the back-to-back configuration. In particular, our experimental tests led with 20 km DSF, and 50 km of SMF+DCM have successfully reduced/compensated the fiber contribution and enabled a cancellation noise figure ranging from 10 to 20 dB. We have also found numerically that fiber channel nonlinear effects contributes up to a few negligible pourcent to the cancellation-to-chaos ratio, when proper dispersion compensation is achieved. This numerically found contribution is compatible with the actually obtained minimum experimental value of the cancellation-to-chaos ratio. Finally, Fig. 8 shows the results of numerical simulations for the eye diagram of a 8 Gbs/s message decoded after propagation by a receiver with a mismatch of 5% in τ and 10% in G. When fiber dispersion effects are compensated or a DSF is used the message can be clearly recovered.

These results thereby indicate that our phase chaos cryptosystem can be integrated in standard optical fiber networks where such dispersion management schemes are actually implemented. Moreover dispersion sensitivity can be beneficial to enhance chaos communication security, through a secretly set DCM inside the chaos generation process.

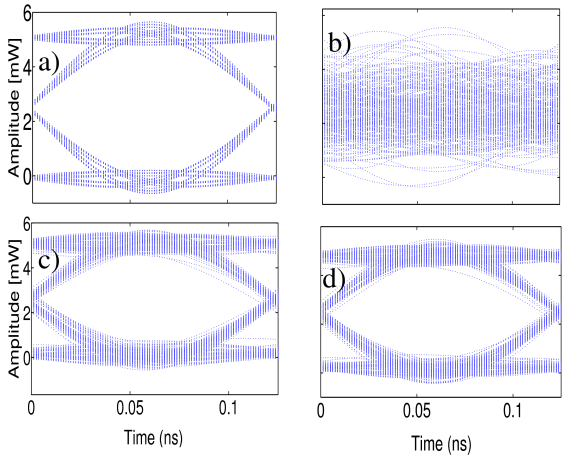

Fig. 8. (Color online) Numerical eye diagrams for a) the original message [17] and the recovered one $\mu_r(t)$ after propagation over b) 21 km of SMF (as in Fig. 5), c) 50 km of SMF and 5 km of DCF (as in Fig. 6) and d) 55 km of DSF (as in Fig. 7).

References

[1] K. M. Cuomo and A. V. Oppenheim, "Circuit implementation of synchronized chaos with applications to communications", *Phys. Rev. Lett.* vol. **71**, pp. 65–68, 1993.

[2] S. Donati and C. R. Mirasso, Guest Editors, "Special issue on optical chaos and applications to cryptography", *IEEE J. Quantum Electron.*, vol. **38**, no. 9, Sept. 2002.

[3] A. Argyris, D. Syvridis, L. Larger, V. Annovazzi-Lodi, P. Colet, I. Fischer, J. Garcia-Ojalvo, C. R. Mirasso, L. Pesquera and K. A. Shore, "Chaos-based communications at high bit rates using commercial fibre-optic links", *Nature*, vol. **438**, pp. 343–346, 2005.

[4] R. Lavrov, M. Peil, M. Jacquot, L. Larger, V. Udaltsov, and J. Dudley, "Electro-optic delay oscillator with nonlocal nonlinearity: optical phase dynamics, chaos, and synchronization", *Phys. Rev. E* vol. **80**, pp. 026207-1–9, 2009.

[5] R. Lavrov, M. Jacquot, and L. Larger "Nonlocal nonlinear electro-optic phase dynamics demonstrating 10 Gb/s chaos communications" *IEEE J. Quantum Electron.*, to appear 2010.

[6] L. Larger, J.-P. Goedgebuer, and F. Delorme, "Optical encryption system using hyperchaos generated by an optoelectronic wavelength oscillator", *Phys. Rev. E*, vol. **57**, pp. 6618–6624, 1998.

[7] Y. Chembo Kouomou, P. Colet, N. Gastaud, and L. Larger, "Effect of parameter mismatch on the synchronization of chaotic semiconductor lasers with electrooptical feedback", *Phys. Rev. E*, vol. **69**, pp. 056226-1–15, 2004.

[8] Y. Chembo Kouomou, P. Colet, L. Larger, and N. Gastaud, "Mismatch-induced bit error rate in optical chaos communications using semiconductor lasers with electrooptical feedback", *IEEE J. Quantum Electron.*, vol. **41**, no. 2, pp. 156–163, 2005.

[9] N. Gastaud, S. Poinsot, L. Larger, J.-M. Merolla, M. Hanna, J.-P. Goedgebuer and F. Malassenet, "Electro-optical chaos for multi-10 Gbit/s optical transmissions", *Electron. Lett.* , vol. **40**, pp. 898–899, 2004.

[10] S. F. Yu, P. Shum, and N. Q. Ngo, "Performance of optical communication systems using multimode vertical cavity surface emitting lasers", *Opt. Commun.*, vol. **200**, pp. 143–152, 2001.

[11] A. Sanchez-Diaz, C. R. Mirasso, P. Colet, and P. Garcia-Fernandez, "Encoded Gbit/s digital communications with synchronized chaotic semiconductor lasers", *IEEE J. Quantum Electron.*, vol. **35**, no. 3, pp. 292–297, 1999.

[12] A. Bogris, D. Kanakidis, A. Argyris, and D. Syvridis, "Performance characterization of a closed-loop chaotic communication

system including fiber transmission in dispersion shifted fibers", *IEEE J. Quantum Electron.*, vol. **40**, no. 9, pp. 1326–1336, 2004.
[13] D. Kanakidis, A. Bogris, A. Argyris, and D. Syvridis, "Numerical investigation of fiber transmission of a chaotic encrypted message using dispersion compensation schemes", *IEEE J. Lightwave Technol.*, vol. **22**, no. 10, pp. 2256–2263, 2004.
[14] A. Argyris, E. Grivas, M. Hamacher,A. Bogris, and D. Syvridis, "Chaos-on-a-chip secures data transmission in optical fiber links" *Optics Express*, vol. **18**, pp. 5188–5198, 2010.
[15] G. P. Agrawal, "Nonlinear fiber optics", 4^{th} edition, Academic press, 2007.
[16] Experimental spectra decay faster than numerical ones because the experimental filter is of higher order.
[17] The decoded message μ_r is to be compared with the input message going through an equivalent detection scheme involving a MZI with delay δT_m. Therefore Fig. 8 a) shows $\frac{1}{4}SP_0|e^{im(t)} + e^{im(t-\delta T_m)}|^2$.